Effect of Heat Transfer on Materials Selection for Bimaterial Electrothermal Actuators

Prasanna Srinivasan and S. Mark Spearing, *Member, ASME*

***Abstract*—Bimaterial electrothermal actuation is a commonly employed actuation method in microsystems. This paper focuses on optimal materials selection for bimaterial structures to maximize the thermomechanical response based on electrothermal heat-transfer analysis. Competition between different modes of heat transfer in electrothermally actuated cantilever bimaterial is analyzed for structures at the microscale ($10\ \mu\text{m} \leq L \leq 1$ mm) using a lumped heat-capacity formulation. The choice of materials has a strong influence on the functional effectiveness and the actuation frequency even though the electromechanical efficiency is inherently small ($\sim 10^{-5}$). Frequencies on the order of $\sim$100 Hz to 15 kHz can be obtained for bimaterial structures at small scales by varying either the operating temperature range or the rate of heat dissipation. It is found that engineering alloys/metals perform better than other classes of materials for high-work high-frequency ($\sim$10 kHz) actuation within achievable temperature limits. [2006-0177]**

***Index Terms*—Electrothermal effects, microactuators, resistance heating, scaling and materials selection, thermomechanical.**

I. Introduction

MATERIALS selection is a critical step in the design cycle of any engineering system. The selection of materials for microelectromechanical system (MEMS) is complicated by the highly integrated multifunctional roles of the components. Seldom will a material have properties delivering maximum performance in all the governing physical domains. The conventional set of MEMS materials [1], although compatible with existing micromachining methods, are not an optimal choice for the maximum performance. This represents an opportunity to expand the MEMS materials set in order to improve the functionality of devices.

Bimaterial electrothermal (BET) actuation is a commonly employed actuation method due to simplicity in the micromachining processes and its ability to provide out-of-plane actuation, which is, otherwise, difficult to achieve. There have been few published works on electrothermal heat transfer in microsystems, which include the following: 1) estimation of the time constant and lateral resonances of Al–Si bimaterial [2] for resonant sensors and microswitches applications, 2) evaluation of the buckling characteristics of micromachined polysilicon beams [3] under thermal load using electrothermal and thermoelastic studies, 3) experimental investigation of the electrothermal behavior of a diamond-like carbon (DLC)–Ni microcage device for handling living biological cells [4], 4) estimation of the temperature field in an SU8-Pt polymeric microgripper [5] by numerical simulations, 5) evaluation of the transient thermal field of an Au–Si microcantilever actuated by a laser pulse for wireless MEMS applications [6], and 6) effect of electrical/thermal properties on the temperature of silicon microcantilevers used in atomic-force microscopy for nanotopographic measurements [7]. These works analyzed the performance of the specific BET actuators employed in different microsystems for various applications. However, a more generalized electrothermal analysis to guide the materials selection for such actuators has not been previously attempted. This paper aims to identify promising candidates for BET actuators at small scales ($10\ \mu\text{m} \leq L \leq 1$ mm) by building on previous works focused on the overall selection of actuation principles, at the macro [8] and microscales [9].

The key performance metrics for BET actuators are the displacement (slope), force (moment), work per cycle, the actuation frequency, and the effectiveness. This paper discusses a strategy for selecting suitable candidate materials for bimaterial structures based on electrothermal heat-transfer analyses in order to improve the performance. The process of materials selection explained in this paper follows previous work, where displacement, force, and work/volume of the actuators were maximized for a constant uniform temperature difference [10]. Therefore, the resulting set of materials identified in these two studies would be promising candidates for BET actuators. The objective of this paper is to develop an analytical framework for materials selection for BET actuators considering electrothermal heat-transfer effects.

The relevant performance metrics for BET actuators which depend on the heat-transfer response are the frequency, effectiveness, and electromechanical efficiency. A high actuation frequency is required for applications such as micromirror positioners [11], microgrippers, fiber-optic switches [12], and boundary-layer flow-control devices. Effectiveness is a measure of displacement/force/work achieved within a cycle per unit electrical energy consumed. The characteristic electromechanical efficiency is defined here as the ratio of the total mechanical work done by the actuator to the electrical energy supplied.

The competition between different modes of heat transfer which constitutes the total heat dissipation varies according to the actuator scales. This variation in the competing heat-transfer modes affects the thermomechanical response of the actuators. The effect of scaling and its influence on the response

Manuscript received August 24, 2006. The work of P. Srinivasan was supported in part by the Overseas Research Students Awards Scheme and in part by the University of Southampton, U.K. Subject Editor N. de Rooij.

The authors are with the School of Engineering Sciences, University of Southampton, SO171BJ Southampton, U.K. (e-mail: prasanna@soton.ac.uk; spearing@soton.ac.uk).

Digital Object Identifier 10.1109/JMEMS.2008.918617

which eventually determines the materials selection is therefore addressed.

This paper is organized as follows. Section II gives an overview of the thermomechanical design of BET actuators. Section III discusses the evaluation of the equivalent thermal properties of a bimaterial. Evaluation of the steady state and transient thermal responses of a bimaterial are presented in Sections IV and V, respectively. Section VI discusses the estimation of the functional effectiveness and the electromechanical efficiency of a bimaterial. Section VII illustrates the application of thermal models for materials selection. Section VIII discusses the materials selection process and the influence of scaling on the selection process. Section IX provides concluding remarks drawn from this study.

II. Overview of the Thermomechanical Design of a BET Actuator

Fig. 1 shows a schematic of an electrothermally actuated bimaterial. The relevant material properties are Young's modulus (E), thermal-expansion coefficient (α), thermal conductivity (K), thermal emissivity (ε), specific-heat capacity (C), and density (ρ). The subscripts correspond to the material layers 1 and 2, respectively. The thicknesses of the two layers are t_1 and t_2, respectively. The width of the beam is b, and its length is L. The base and ambient temperatures are T_b and T_∞, respectively. Using Timoshenko bimetallic strip theory [13], the relevant performance metrics which gauge the thermomechanical response, namely, free-end slope (Θ), blocked moment (M), and work done per volume (W) were developed [14]

$$\Theta = \frac{6L(\Delta\alpha)(\Delta T)}{t\left(3+\left(\frac{(1+\lambda\xi)(1+\xi^3\lambda)}{\lambda\xi(\xi+1)^2}\right)\right)} \tag{1}$$

$$M = \frac{E_1 bt^2(\Delta\alpha)(\Delta T)}{2\left(\frac{(\xi+1)(1+\lambda\xi)}{\xi}\right)} \tag{2}$$

$$W = \frac{3E_1(\Delta\alpha)^2(\Delta T)^2}{8\left(\frac{(1+\lambda\xi)^2(1+\xi^3\lambda)}{\lambda\xi^2(\xi+1)}+\frac{3(1+\lambda\xi)(\xi+1)}{\xi}\right)} \tag{3}$$

where $\lambda = E_1/E_2$ is the ratio of Young's moduli of the bimaterial, $\xi = t_1/t_2$ is the ratio of the thicknesses of the two layers, $\Delta\alpha = \alpha_1 - \alpha_2$ is the difference between the thermal-expansion coefficients of the bimaterial, and $\Delta T = T - T_\infty$ is the difference between the nominal temperature of the bimaterial T and the ambient temperature T_∞. A strategy for selecting optimal material pairs which deliver maximum thermomechanical performance for a constant ΔT was previously developed [14]. The optimality condition pertaining to the maximum steady-state thermomechanical response of a bimaterial is given as

$$\lambda\xi_o^2 = 1 \tag{4}$$

where ξ_o is the optimal thickness ratio corresponding to the maximum thermomechanical response for a given pair of materials. Substituting (4) in (1), (2), and (3) gives the optimal thermomechanical response

$$\Theta_o = \frac{3L(\Delta\alpha)(\Delta T)}{2t} = \frac{\Theta_{no}L(\Delta T)}{t} \tag{5}$$

$$M_o = \frac{E_1 bt^2(\Delta\alpha)(\Delta T)}{2\left(\frac{1+\xi_o}{\xi_o}\right)^2} = M_{no}bt^2(\Delta T) \tag{6}$$

$$W_o = \left(\frac{3E_1(\Delta\alpha)^2(\Delta T)^2}{32}\right)\left(\frac{\xi_o}{1+\xi_o}\right)^2 = W_{no}(\Delta T)^2 \tag{7}$$

where Θ_o, M_o, and W_o are the optimal thermomechanical responses for a given pair of materials. Θ_{no}, M_{no}, and W_{no} are material parameters which correspond to the optimal slope, moment, and work normalized with respect to geometry and temperature. The variable ΔT is a non-linear function of electrical and thermal properties of the materials employed for a given geometry. Since for an optimal response, the ratio of thicknesses of the bi-layers is a function of the elastic moduli ratio of the bi-material as given in (4), it is possible to express ΔT as a function of mechanical, electrical, and thermal properties. This paper investigates the influence of the competing heat-transfer modes on ΔT, which in turn affects the thermomechanical response of the bimaterial.

A BET actuator is a microscale structure with in-plane dimensions in the range of 10–1000 μm. Actuation is typically achieved by resistive heating followed by uncontrolled cooling. The small scale allows a lumped heat-capacity formulation to be used, as the surface convective resistance is large as compared to the internal conduction resistance. This is quantified by the Biot number (Bi) [15]

$$Bi = \frac{hL_c}{K_{eq}} \tag{8}$$

where $L_c = V/A_s$ is the characteristic length, which is given by the ratio of the volume, V to the surface area, A_s of the actuator, K_{eq} is the equivalent thermal conductivity of the actuator materials, and h is the heat-transfer coefficient of the actuator surface. The surface area to the volume ratio for microscale structures is usually very large, and therefore, the Biot number is very small ($\sim$0.01–0.1), which justifies the use of a lumped heat-capacity model.

III. Evaluation of Equivalent Thermal Properties

From (4), it is clear that the optimal thickness ratio of the bimaterials depends only on the ratio of the Young's moduli and is independent of the thermal-expansion coefficients of the materials. Therefore, the equivalent thermal properties of a bimaterial with an optimal thickness ratio also depend on the Young's moduli of the bimaterials. The equivalent thermal properties relevant to the present analysis are thermal conductivity, volumetric thermal capacity, and thermal emissivity.

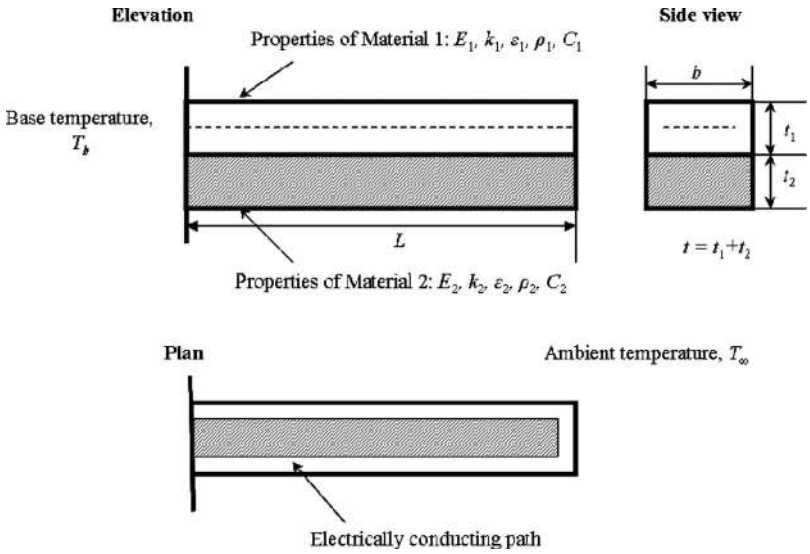

Fig. 1. Schematic of a cantilever bimaterial heated electrically.

Furthermore, the power generated per unit volume due to Joule heating also must be evaluated for the thermal analysis.

A. Equivalent Thermal Conductivity K_{eq}

The equivalent thermal conductivity K_{eq} is defined as the property of an equivalent homogenous material of unit thickness and unit area of cross section, which, when maintained under a unit thermal gradient, would transfer the same energy as the bimaterial layers under the same conditions, giving

$$K_{\mathrm{eq}} = \frac{K_1\xi_{\mathrm{o}} + K_2}{1 + \xi_{\mathrm{o}}}. \tag{9}$$

B. Equivalent Volumetric Thermal Capacity $(\rho C)_{\mathrm{eq}}$

The equivalent thermal capacity $(\rho C)_{\mathrm{eq}}$ is similarly defined

$$(\rho C)_{\mathrm{eq}} = \frac{(\rho_1 C_1)\xi_{\mathrm{o}} + (\rho_2 C_2)}{\xi_{\mathrm{o}} + 1}. \tag{10}$$

C. Equivalent Emissivity $\varepsilon_{\mathrm{eq}}$

The equivalent emissivity $\varepsilon_{\mathrm{eq}}$ is defined as the property of an equivalent homogenous material which would emanate the same amount of radiation from its surface when maintained at a given temperature as the bimaterial layers under the same conditions, i.e.,

$$\varepsilon_{\mathrm{eq}} = \frac{\varepsilon_1(b + t_1) + \varepsilon_2(b + t_2)}{b + t}. \tag{11}$$

D. Power Generated Per Volume Q_{v}

The heating element in the actuator is usually one of the bimaterial layers; typically, the one which requires least voltage for generating a large heating current. Silicon, being the most commonly employed substrate material in microsystems, is often considered as the heating element, because its electrical resistivity can be varied over a wide range (10^3–$10^{-7}\ \Omega \cdot \mathrm{m}$) by doping with boron [16]. The electrical conducting path runs along the U-shaped heating element, as shown in Fig. 1. End effects are ignored, and the length of the conductor is assumed to be $2L$. The power generated per unit volume of the actuator when heated by a constant-voltage source is given as

$$Q_{\mathrm{v}} = \frac{V^2}{4\varphi L^2(1 + 1/\xi_{\mathrm{o}})} \tag{12}$$

where V is the constant actuation voltage used for Joule heating and φ is the resistivity of the heating element. The effect of any insulating oxide layer sandwiched between the bimaterial layers is ignored in the present analysis.

IV. Steady-State Temperature Field of a Bimaterial

Fig. 2(a) shows a 1-D heat-transfer model of a cantilever beam with equivalent thermal properties heated electrically by a constant voltage V. The base which acts as a heat sink is maintained at a constant temperature T_{b}, and the ambient temperature is T_∞. The cross-sectional area of the beam is A, and the perimeter of the cross section is P. The total heat generated due to electrical heating is dissipated by conduction, convection, and radiation. The heat transfer at the free end of the beam at $x = L$ is negligible and, therefore, is modeled as a thermally insulated section.

Consider an elemental control volume with the temperature T at distance of x from the base. Let dT be the temperature change over the length dx. Fig. 2(b) shows the energy flow across the control volume considered. The total thermal energy generated within the control volume is dissipated by diffusion to the base, convection to the surrounding fluid medium, and radiation. Using the energy-balance relation, an expression for

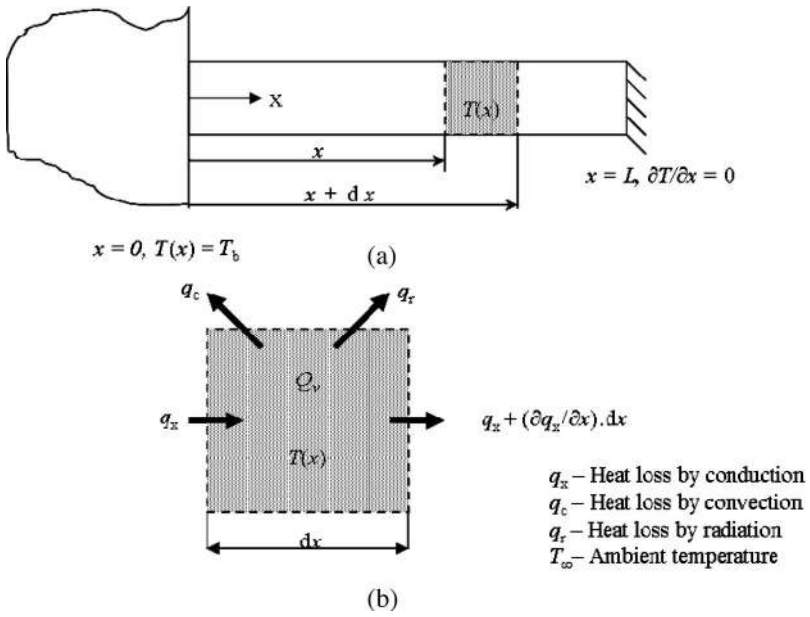

Fig. 2. (a) Thermal model of a cantilever bimaterial. (b) Energy flow across the control volume considered.

the temperature field $T(x)$ along the length of the beam is obtained with/without convection and radiation effects

$$T(x) - T_{\mathrm{b}} = \left(\frac{xQ_{\mathrm{v}}}{K_{\mathrm{eq}}}\right)\left(L - \frac{x}{2}\right) \tag{13}$$

is the temperature field without taking into account convection/radiation effects

$$\left(\frac{T(x) - \left(T_\infty + \dfrac{Q_{\mathrm{v}}}{K_{\mathrm{eq}}m^2}\right)}{T_{\mathrm{b}} - \left(T_\infty + \dfrac{Q_{\mathrm{v}}}{K_{\mathrm{eq}}m^2}\right)}\right) = \frac{\cosh m(L-x)}{\cosh mL} \tag{14}$$

is the temperature field considering the convection/radiation effects. The variable $m = \sqrt{h_{\mathrm{t}}P/K_{\mathrm{eq}}A}$, $h_{\mathrm{t}} = h_{\mathrm{c}} + \sigma\varepsilon_{\mathrm{eq}}(T(x)^2 + T_\infty^2)(T(x) + T_\infty)$ is the overall heat-transfer coefficient, h_{c} is the convective heat-transfer coefficient, and $\sigma = 5.67 \times 10^{-8}$ W/m$^2 \cdot$K^4 is the Stefan–Boltzmann constant. The characteristic temperature of the bimaterial is defined by the average temperature, T_{av} along its length, which is given by

$$T_{\mathrm{av}} - T_{\mathrm{b}} = \frac{L^2Q_{\mathrm{v}}}{3K_{\mathrm{eq}}} \tag{15}$$

in the absence of convection/radiation effects

$$\left(\frac{T_{\mathrm{av}} - \left(\dfrac{T_\infty + Q_v}{K_{\mathrm{eq}}m_{\mathrm{av}}^2}\right)}{T_{\mathrm{b}} - \left(T_\infty + \dfrac{Q_v}{K_{\mathrm{eq}}m_{\mathrm{av}}^2}\right)}\right) = \frac{\tanh m_{\mathrm{av}}L}{m_{\mathrm{av}}L} \tag{16}$$

is the average temperature considering the convection/radiation effects. The variable m_{av} is the value of m at $T(x) = T_{\mathrm{av}}$.

Using (15), a parameter called the electrothermal power index P_I is defined considering the heat dissipation due to conduction

$$P_{\mathrm{I}} = \frac{1}{3K_{\mathrm{eq}}} = \left(\frac{(T_{\mathrm{av}} - T_{\mathrm{b}})}{Q_{\mathrm{v}}L^2}\right) \approx \frac{(\Delta T)}{Q_{\mathrm{v}}L^2}. \tag{17}$$

P_{I} is a material-dependent parameter, which gives a measure of the achievable temperature for a bimaterial of fixed length when heated by a source generating unit power per volume of the material. Since materials selection is generally based on the relative estimates of the performance, convective effects are ignored in the evaluation of the P_{I} as they do not have any bearing on the selection criteria.

V. Transient Thermal Response of a Bimaterial

The frequency of BET actuators depends on the time taken by the actuators to heat and cool alternately between the prescribed operating temperatures. The time taken by the actuators to be heated to a given temperature can be controlled to a certain extent by altering the electrical resistivity of the heating element (e.g., silicon) by doping. The cooling phase is usually uncontrolled, and it depends on the thermal properties of the substrate materials. If T_{p} and T_{v} are the operating temperatures of a bimaterial with $T_{\mathrm{p}} > T_{\mathrm{v}}$, then the time corresponding to heating (t_{h}) and cooling (t_{c}) phases can be obtained by solving the implicit transient thermal model using numerical integration

$$T^{\mathrm{i}+1} = \frac{T^{\mathrm{i}} + F_{\mathrm{o}}\left(T_{\mathrm{b}} + BiT_\infty + \left(\frac{Q_{\mathrm{vt}}L^2}{K_{\mathrm{eq}}}\right)\right)}{1 + F_{\mathrm{o}}(Bi + 1)} \tag{18}$$

correspond to heating phase

$$T^{\mathrm{i}+1} = \frac{T^{\mathrm{i}} + F_{\mathrm{o}}(T_{\mathrm{b}} + BiT_\infty)}{1 + F_{\mathrm{o}}(Bi + 1)} \tag{19}$$

correspond to cooling phase. T^{i} and $T^{\mathrm{i}+1}$ are the temperatures of the bimaterial at the successive instants t and $t+\Delta t$, Q_{vt} is the constant electrothermal power generated per unit volume during the heating phase, $F_{\mathrm{o}} = K_{\mathrm{eq}}\Delta t/(\rho C)_{\mathrm{eq}}L^2$ is the Fourier number, and $Bi = h_{\mathrm{t}}PL^2/K_{\mathrm{eq}}A$ is the Biot number.

The losses associated with the heating phase for a high constant electrothermal power generation per unit volume ($Q_{\mathrm{vt}} \sim 10^{12}-10^{13}$ W/m^3) is usually low ($< 0.1\ \mathrm{Q_{vt}}$). As a result, the electrical energy supplied can be assumed to be equal to the internal thermal energy stored within the bimaterial. Therefore, for a linear ramp up from T_{v} to T_{p}, the transient thermal response corresponding to the heating phase given by (18) reduces to

$$Q_{\mathrm{vt}} \approx \frac{(\rho C)_{\mathrm{eq}}(T_{\mathrm{p}} - T_{\mathrm{v}})}{t_{\mathrm{h}}}. \tag{20}$$

Since the electrothermal heating rate is faster than the cooling rate ($\sim 10-100\times$), it can be ignored in the computation of the cyclic frequency. The characteristic actuation frequency can thus be evaluated as

$$f \approx \frac{1}{t_{\mathrm{c}}}. \tag{21}$$

Assuming that $t_{\mathrm{h}} = 1/(10f)$, the electrothermal power generated per unit volume of the bimaterial during heating phase can be evaluated from (20) in terms of the actuation frequency.

$$Q_{\mathrm{vt}} = 10f(\rho C)_{\mathrm{eq}}(T_{\mathrm{p}} - T_{\mathrm{v}}). \tag{22}$$

It should be noted that the actuation frequency depends on the operating temperatures T_{p} and T_{v} for the given pair of materials and the length scale.

VI. Effectiveness and Efficiency of the BET Actuator

A thermomechanical design criterion, which governs materials selection for many BET actuators, is the displacement/force/work per cycle achieved for the given amount of electrical energy supplied. Therefore, the effectiveness of BET actuators is quantified here based on the optimal displacement/force/work per cycle achieved from a given pair of materials for unit electrical energy consumed. The effectiveness can be either displacement (slope) based Θ_{eff}, force (moment) based M_{eff}, or work based W_{eff}. Designing an actuator with the required effectiveness is determined by the functional requirements. Using (5)–(7) for the effectiveness of the BET actuators are obtained

$$\Theta_{\mathrm{eff}} = \frac{\Theta_{\mathrm{o}}}{Q_{\mathrm{v}}Lbt} = \frac{\Theta_{\mathrm{no}}(\Delta T)}{bt^2Q_{\mathrm{v}}} \tag{23}$$

$$M_{\mathrm{eff}} = \frac{M_{\mathrm{o}}}{Q_{\mathrm{v}}Lbt} = \frac{M_{\mathrm{no}}t(\Delta T)}{Q_{\mathrm{v}}L} \tag{24}$$

$$W_{\mathrm{eff}} = \frac{M_{\mathrm{eff}}\Theta_{\mathrm{eff}}}{8} = \frac{W_{\mathrm{no}}(\Delta T)^2}{Q_{\mathrm{v}}^2Lbt}. \tag{25}$$

Effectiveness can also be regarded as the performance of the actuator within a cycle. Substituting (17) in (23)–(25), effectiveness can be obtained in terms of the mechanical/thermal properties of the bimaterial

$$\Theta_{\mathrm{eff}} = \frac{\Theta_{\mathrm{no}}(\Delta T)}{bt^2Q_{\mathrm{v}}} = \frac{(\Delta\alpha)L^2}{2K_{\mathrm{eq}}bt^2} \tag{26}$$

$$M_{\mathrm{eff}} = \frac{M_{\mathrm{no}}t(\Delta T)}{Q_{\mathrm{v}}L} = \frac{E_1(\Delta\alpha)Lt}{6\left(\frac{1+\xi_{\mathrm{o}}}{\xi_{\mathrm{o}}}\right)^2 K_{\mathrm{eq}}} \tag{27}$$

$$W_{\mathrm{eff}} = \frac{W_{\mathrm{no}}(\Delta T)^2}{Q_{\mathrm{v}}^2Lbt} = \frac{E_1(\Delta\alpha)^2L^3}{96\left(\frac{1+\xi_{\mathrm{o}}}{\xi_{\mathrm{o}}}\right)^2 K_{\mathrm{eq}}^2bt}. \tag{28}$$

By normalizing (26), (27), and (28) with respect to geometry, indices for effectiveness based on the displacement, force, and work per cycle can be obtained

$$\Theta_{\mathrm{EI}} = \frac{\Theta_{\mathrm{eff}}bt^2}{L^2} = \frac{(\Delta\alpha)}{2K_{\mathrm{eq}}} \tag{29}$$

$$M_{\mathrm{EI}} = \frac{M_{\mathrm{eff}}}{Lt} = \frac{E_1(\Delta\alpha)}{6K_{\mathrm{eq}}\left(\frac{1+\xi_{\mathrm{o}}}{\xi_{\mathrm{o}}}\right)^2} \tag{30}$$

$$W_{\mathrm{EI}} = \frac{W_{\mathrm{eff}}bt}{L^3} = \frac{E_1(\Delta\alpha)^2}{96K_{\mathrm{eq}}^2\left(\frac{1+\xi_{\mathrm{o}}}{\xi_{\mathrm{o}}}\right)^2} \tag{31}$$

where Θ_{EI}, M_{EI}, and W_{EI} are indices for effectiveness based on slope, moment, and work, respectively, for a fixed geometry of actuator.

The candidate materials selected besides being functionally effective should also be efficient in performance. Therefore, the electromechanical efficiency η_{em} is defined here as the ratio of the optimal mechanical-power output to the electrical-power input for a given pair of materials, i.e.,

$$\eta_{\mathrm{em}} = \frac{P_{\mathrm{av}}}{Q_{\mathrm{vt}}} = \frac{P_{\mathrm{av}}}{10f(\rho C)_{\mathrm{eq}}(T_{\mathrm{p}} - T_{\mathrm{v}})} \tag{32}$$

where $P_{\mathrm{av}} = (1/(\Delta t))\int_t^{t+\Delta t} |dW_{\mathrm{o}}/dt|dt$ is the average mechanical-power output, which depends on the transient thermal response of the bimaterial during the cooling phase for the temperature difference achieved with the given amount of electrical power supplied. The choices of materials which are functionally effective are not necessarily efficient, because η_{em} depends on the rate at which the thermal energy is dissipated by the bimaterial for the achievable temperature difference due to the electrical energy supplied.

VII. Thermal Considerations in the Materials Selection

The competition between the different modes of heat transfer which contribute to the thermal-energy dissipation varies with the length scale of the bimaterial structure. As a consequence, the thermomechanical response affecting the materials selection will also depend on scale (10 μm to 1 mm). Hence,

TABLE I
PROPERTIES OF SINGLE-CRYSTAL SILICON

Young's Modulus, E_1 = 165 GPa
Thermal conductivity, K_1 = 150 W/mK
Thermal expansion coefficient, α_1 = 2.49 μm/mK
Electrical resistivity, φ= 10^{-4} Ω-m
Specific heat capacity, C_1 = 700 J/kg K
Density, ρ_1 = 2280 kg/m^3

the performance of different classes of materials on a given substrate is examined as function of scale to identify promising candidates.

Silicon is one of the most commonly preferred substrate materials for microsystems due to its wide availability and ease of microfabrication besides having favorable properties in the various physical domains. For illustration, silicon is chosen as one of the bimaterial layers and is also assumed to act as the heat source. Table I shows the properties of single-crystal silicon used for this analysis. The bimaterial is assumed to be actuated using a constant dc-voltage source. The heat generated by the bimaterial is dissipated by diffusion to the base and convection to the surrounding fluid medium. The temperature of the base is assumed to be at $T_\mathrm{b} = 50\ ^\circ\mathrm{C}$, and the ambient at $T_\infty = 20\ ^\circ\mathrm{C}$. The heat loss by radiation is neglected, which is reasonable, given sensible temperature limits for most materials ($\sim$500 °C). The steady-state thermal field considering the combined effect of conduction and convection depends on the ratio of the perimeter to the area of the cross section, which is a function of thickness of the bimaterial considering $b > t$ for most actuator structures. A conservative estimate of the temperature is therefore obtained by assuming the cross section of the beam to be square with $L/t = 30$. The operating temperature range for most microsystems varies from $\sim$100 °C to 300 °C with the peak temperature not exceeding $\sim$400 °C considering the temperature limits for the different classes of materials at small scale. The operating temperature range is therefore assumed to be 250 °C with the peak temperature $T_\mathrm{p} = 300\ ^\circ\mathrm{C}$ in this paper.

In order to make an effective selection between the candidates, contours of equal response were plotted on an Ashby materials-selection chart [17] in the domain of the governing properties. Materials which lie close to the contours indicating a high response were then considered for further detailed analysis. The materials selection for BET actuators is based on the electrothermal and thermomechanical performances of the bimaterials. Therefore, the performance of different classes of materials on silicon is evaluated on these considerations to identify novel material combinations.

The electrothermal characteristics of different materials can be better understood if contours of P_I are plotted in the domain of relevant properties. Fig. 3(a) shows contours of equal $\log_{10}(P_\mathrm{I})$ plotted in the material domain (E versus K) for silicon. It is evident that P_I for engineering polymers is greater than for engineering alloys/metals on silicon. Therefore, polymers require less power than metals to attain a given temperature. But the voltage required to attain a given temperature varies with the electrical resistance of the heating element, which depends on the electrical resistivity of the substrate materials and the thickness ratio of the bimaterial layers.

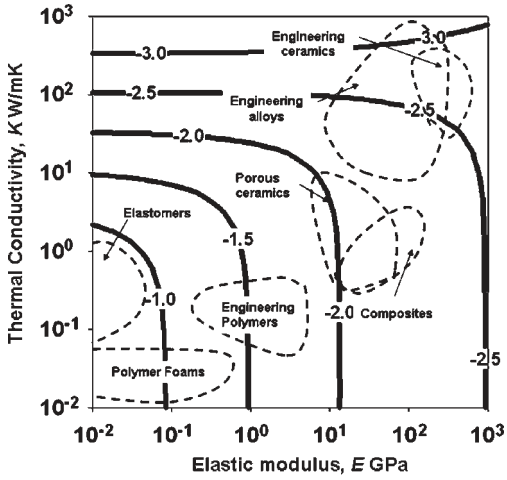

(a)

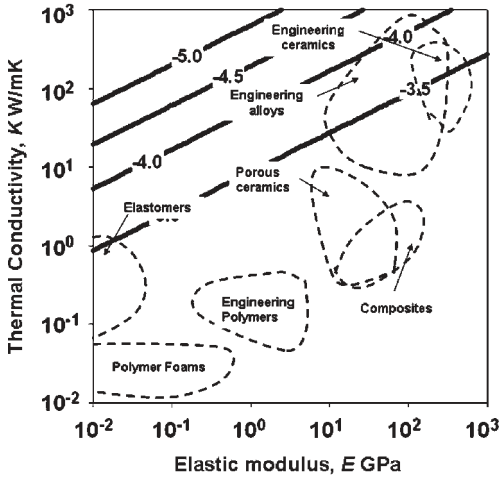

(b)

Fig. 3. Contours of (a) $\log_{10}(P_\mathrm{I})$ and (b) $\log_{10}(V_\mathrm{I})$ for different classes of materials on silicon, which acts as a heat source.

A parameter termed as the electrothermal voltage index (V_I) is defined by eliminating Q_v between (12) and (17)

$$V^2 = \frac{(\Delta T)\varphi}{V_\mathrm{I}} \tag{33}$$

where $V_\mathrm{I} = 1/(12K_\mathrm{eq}(1 + 1/\xi_\mathrm{o}))$ is the voltage index of a material layer for a fixed heat source. The influence of V_I on the actuation voltage is small considering the range of variation in the electrical resistivity of different classes of materials (10^{-9}–$10^{15}\ \Omega \cdot \mathrm{m}$). Polymeric substrates would require much higher voltages than semiconductor and metallic substrates and, therefore, are not preferred heating elements. Furthermore, it is also possible to estimate the actuation voltage for a range of materials on a given heat source. Fig. 3(b) shows contours of $\log_{10}(V_\mathrm{I})$ plotted in the material domain (E versus K) for silicon (which also acts as the heat source). It is clear from the plot that the actuation voltage required to attain a given temperature for different classes of materials on silicon varies only within an order of magnitude ($V_\mathrm{I} : 10^{-3}$–10^{-4} mK/W), although the power required varies by two orders of magnitude ($P_\mathrm{I} : 10^{-1}$–10^{-3} mK/W). Fig. 4(a) and (b) shows similar

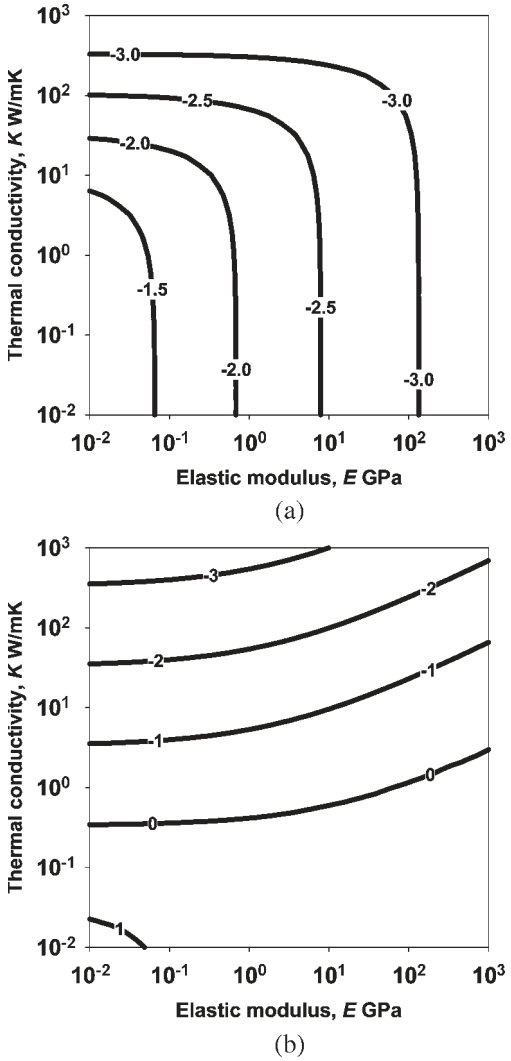

Fig. 4. Contours of equal $\log_{10}(P_{\rm I})$ for materials of different classes on (a) DLC and (b) PMMA substrates.

contours of $\log_{10}(P_{\rm I})$ for DLC and polymethylmethacrylate (PMMA) substrates.

The achievable temperature for different material combinations due to Joule heating can be estimated from the isotherm contours plotted in the relevant material domains considering different modes of heat transfer. Fig. 5 shows steady-state isotherm contours (in Kelvin) obtained using (12) and (15) for different classes of materials on silicon for an optimal thickness ratio $\xi_{\rm o}$, considering heat dissipation due to conduction only. The voltage required for heating was assumed to be 5 V, considering the range of $T_{\rm p}$ preferred for microsystems applications. Fig. 6(a) and (b) shows similar contours for aluminum and PMMA substrates. Although the influence of materials choice on the achievable temperature is dictated by the power supplied, it is also limited further by the failure characteristics of the materials employed (e.g., yield/fracture stress and creep/melting temperature), which are not addressed in this paper. The effect of free convection on the isotherms obtained using (12) and (16) for lengths $L = 100$ μm and 1 mm are shown in Fig. 7(a) and (b), respectively.

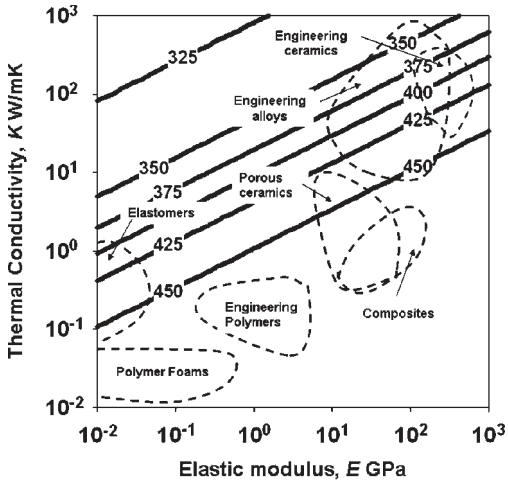

Fig. 5. Comparison of the isotherms for different classes of materials on silicon with Ashby selection chart [17], considering heat dissipation due to conduction ($V = 5$ V).

A macroscale value of the convective heat-transfer coefficient $h_{\rm c} = 10$ W/m$^2 \cdot$K was assumed. Figs. 5 and 7(a) are almost identical, which confirms that conduction is dominant at smaller scales ($L < 1$ mm). The effect of convection becomes apparent at larger scales ($L > 1$ mm), as shown in Fig. 7(b). However, even at this scale, the variation in the isotherms is not very large. Hence, the power dissipated due to convective currents is minimal at a small scale, which further confirms the applicability of the lumped heat-capacity formulation.

The materials-selection strategy for BET actuators is based on complicated tradeoffs between the electrothermal and thermomechanical performances. Therefore, the overall selection criteria for promising candidates depend not only on the electrothermal response (achievable temperature difference for a given pair of materials due to Joule heating by constant voltage) but also on the thermomechanical response (effectiveness and efficiency). Establishing design trades based on the effectiveness is cumbersome due to the interaction between three material properties (E, α, and K). This complexity, however, can be resolved if one of the governing properties is normalized [for example, $(\Delta\alpha)$] and its effect is subsequently superimposed on the resulting response. It is evident from (29) that polymers on silicon are effective in delivering high displacement within a cycle for a given amount of electrical energy expended. Fig. 8 shows contours of equal effectiveness indices for different classes of materials on silicon obtained using (30) and (31) by normalizing with respect to $(\Delta\alpha)$. It is surprising to note from Fig. 8(a) and (b) that polymers are essentially equivalent to engineering alloys/ceramics for delivering high work/force per cycle considering their large thermal-expansion coefficient. However, the large thickness required to compensate for the low Young's modulus may not be acceptable for many applications.

Another important target for materials selection is the electromechanical efficiency, which depends on the maximum mechanical-power output generated from a given amount of electrothermal power supplied, as given by (32). Fig. 9 shows a typical cooling curve for a bimaterial with the prescribed range of operating temperatures. Curve a represents a realistic

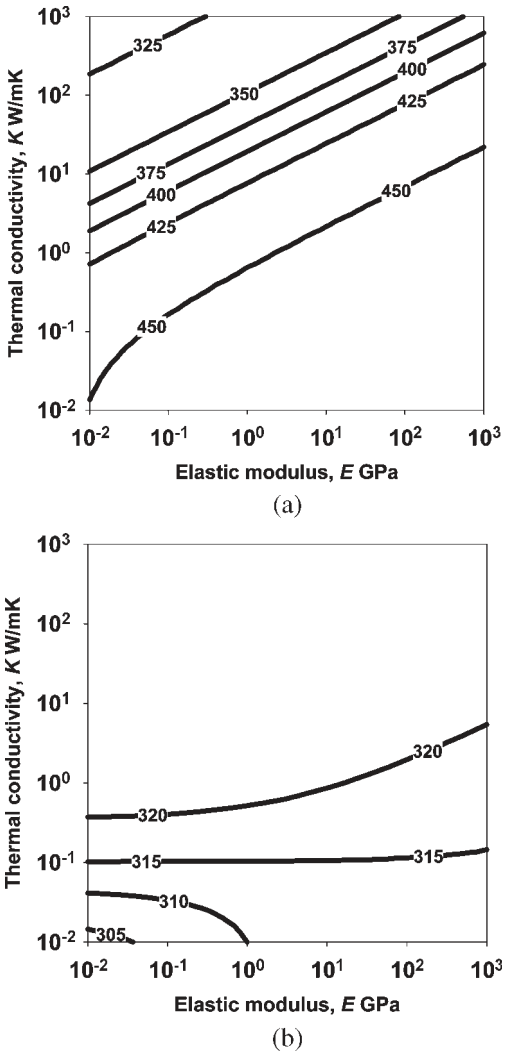

Fig. 6. Steady-state isotherms for different classes of materials on (a) aluminum ($V = 0.1$ V) and (b) PMMA ($V = 5$ V).

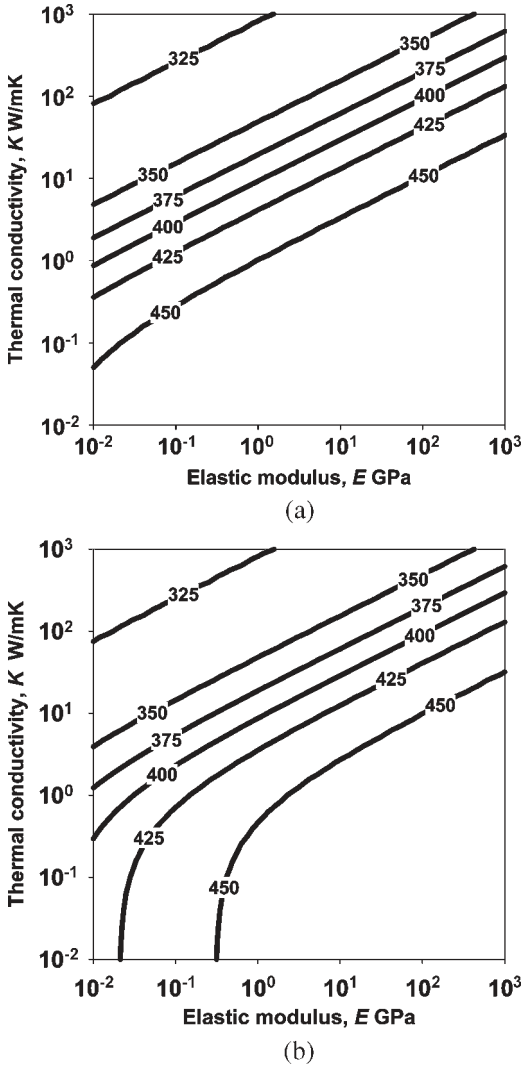

Fig. 7. Isotherms for different classes of materials on silicon considering heat dissipation due to conduction and free convection for (a) $L = 100$ μm and (b) $L = 1$ mm.

transient thermal response of a bimaterial, which can be closely approximated by an exponentially decreasing nonlinear function of time t. The area under the curve bounded by the temperature limits gives a measure of the achievable temperature difference for delivering the work per cycle for a given pair of materials. In order to evolve a relevant closed-form solution for the efficiency metric which guides the materials selection, a linear transient cooling with an instantaneous heating (sawtooth response) is assumed, considering that the losses associated with the heating phase are very low. The equation corresponding to curve b is given as

$$T = T_{\rm p} - (T_{\rm p} - T_{\rm v})ft. \tag{34}$$

Substituting (34) in (32), $\eta_{\rm em}$ for a given material pairs can be obtained

$$\eta_{\rm em} = \frac{W_{\rm no}(T_{\rm p} + T_{\rm v} - 2T_{\infty})}{10(\rho C)_{\rm eq}}. \tag{35}$$

The volumetric specific of different classes of materials is $\sim 10^{6.5}$ J/m$^3 \cdot$ K [17], and therefore, it can be assumed constant. Hence, (35) further reduces to

$$\eta_{\rm em} = \frac{W_{\rm no}(T_{\rm p} + T_{\rm v} - 2T_{\infty})}{10^{7.5}}. \tag{36}$$

Fig. 10 shows contours of equal $\log_{10}(\eta_{\rm em})$ plotted in the domain of $E-\alpha$ for the assumed values of operating temperatures. Since materials from different classes are clustered around $\eta_{\rm em} : 10^{-5}$, it is evident that $\eta_{\rm em}$ for all these materials on silicon is almost constant.

The effect of temperature difference on the actuation frequency can be better understood if a relationship is established between the cooling rate and the operating temperature range. For a linear transient cooling curve from the initial temperature $T_{\rm p}$ to the final temperature $T_{\rm v} < T_{\rm b}$, a relationship can be evolved between the actuation frequency and the operating

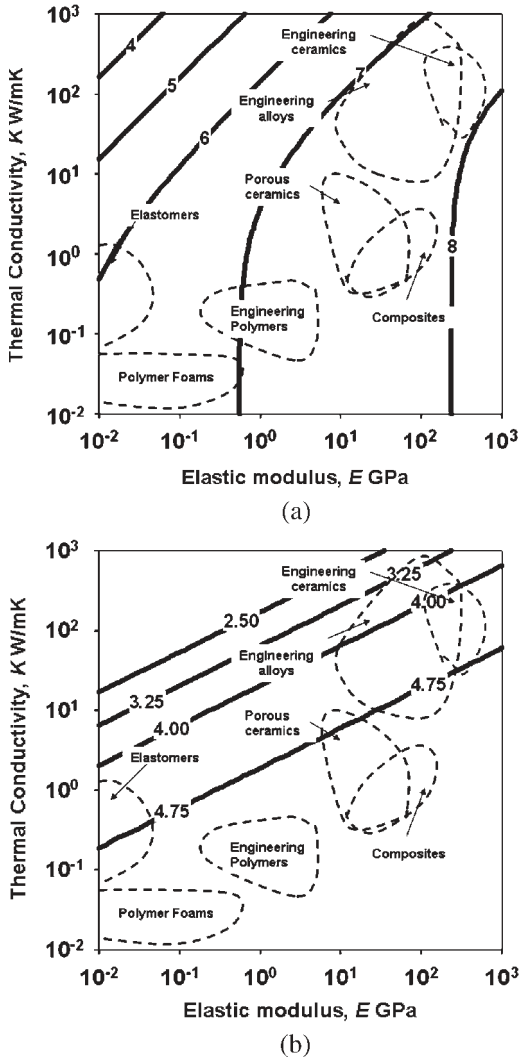

Fig. 8. Contours of effectiveness indices normalized with respect to $(\Delta\alpha)$ for different classes of materials on silicon. (a) Contours of equal $\log_{10}(M_{\rm EI})$. (b) Contours of equal $\log_{10}(W_{\rm EI})$.

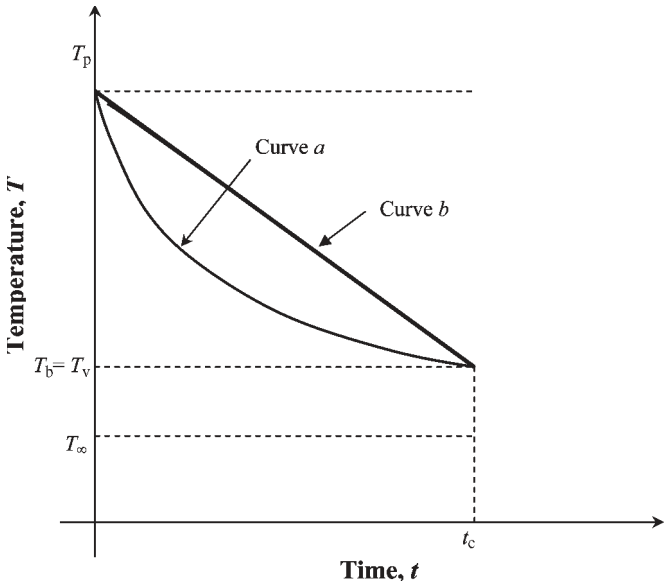

Fig. 9. Typical transient cooling curve of a bimaterial approximated by linear response.

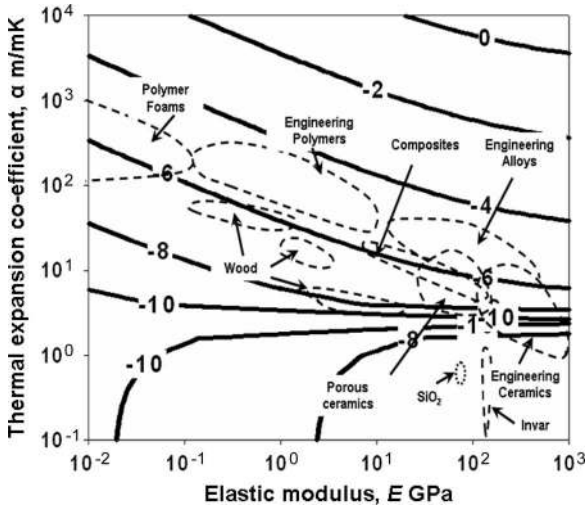

Fig. 10. Contours of equal efficiency $\log_{10}(\eta_{\rm em})$ for different bimaterial combinations with reference to silicon substrate.

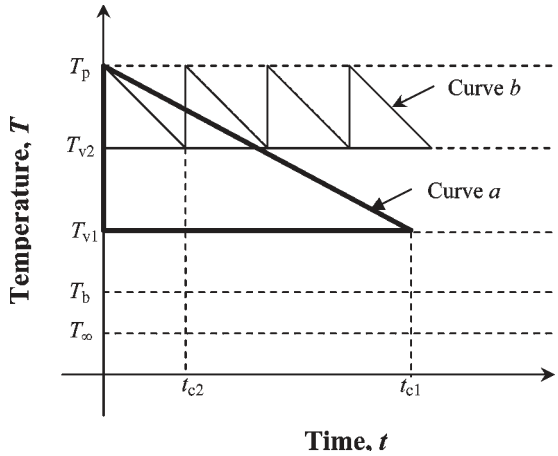

Fig. 11. Effect of operating temperatures on the actuation frequency and the work/volume.

temperatures. Substituting $T^{\rm i} - T^{\rm i+1} = T_{\rm p} - T_{\rm v}$ and $f = 1/\Delta t$, (19) reduces to

$$(T_{\rm p} - T_{\rm v})f = \left(\frac{K_{\rm eq}}{(\rho C)_{\rm eq} L^2}\right)\left((T_{\rm v} - T_{\rm b}) + Bi(T_{\rm v} - T_\infty)\right). \tag{37}$$

Fig. 11 shows two curves a and b, which correspond to two different lower operating temperatures $T_{\rm v1}$ and $T_{\rm v2}$ for a constant peak operating temperature $T_{\rm p}$. The slope of the curves $(-(T_{\rm p} - T_{\rm v})f)$ depends on the thermal diffusivity of the materials chosen and the length scale for a given set of operating temperatures. It is also evident from (37) that the actuation frequency can be increased either by decreasing the operating temperature range or by decreasing the actuator's length. However, in either case, the increase in frequency is compensated for a corresponding drop in the work per cycle, as shown in Fig. 11.

Fig. 12(a) and (b) shows contours of equal actuation frequency for a range of materials on silicon plotted in the domain of governing properties (K versus ρC) at small ($L = 100\ \mu$m) and large ($L = 1$ mm) scales, respectively, using (19) and (21).

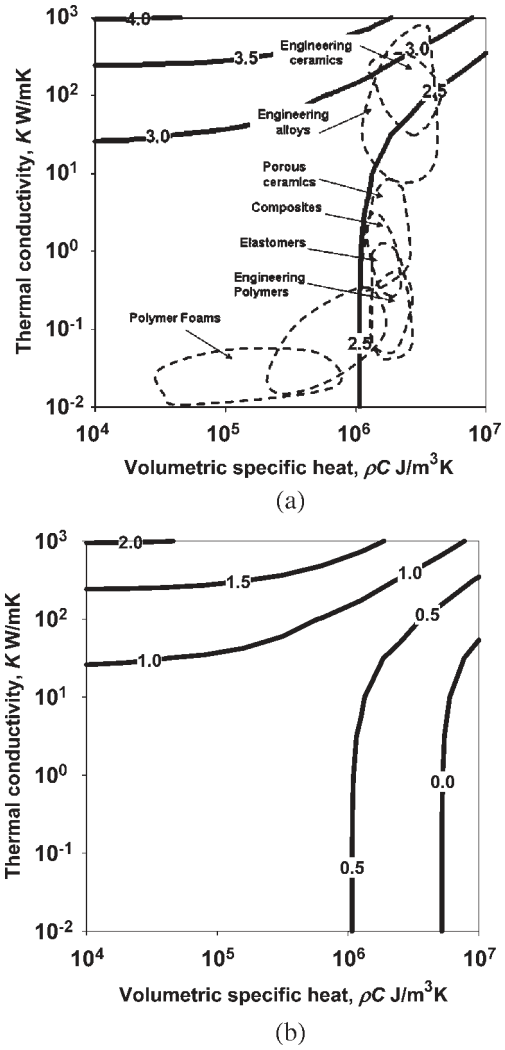

Fig. 12. Contours of equal actuation frequency $\log_{10}(f)$ for different classes of materials on silicon for (a) $L = 100$ μm and (b) $L = 1$ mm at $\xi = 0.5$.

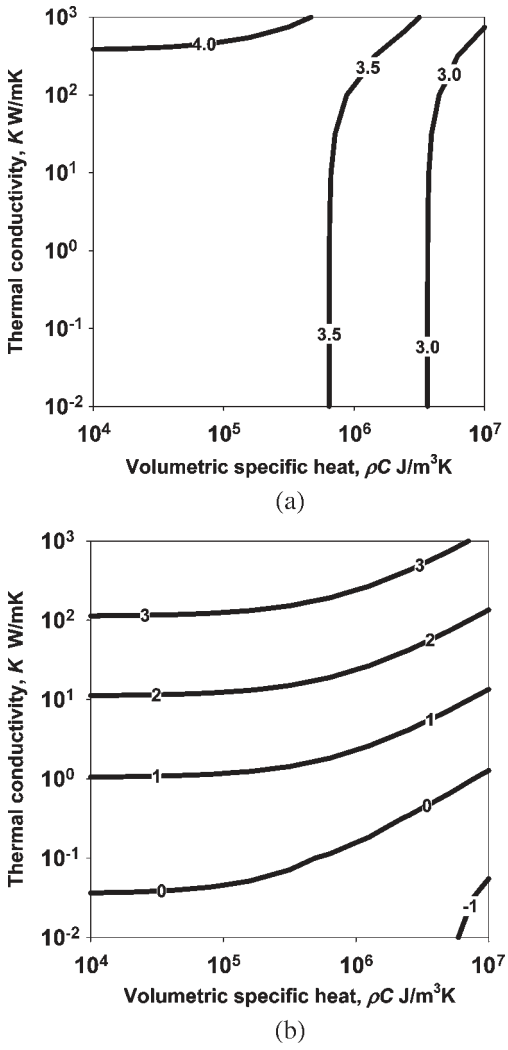

Fig. 13. Contours of equal actuation frequency $\log_{10}(f)$ for different classes of materials on (a) DLC substrate and (b) PMMA substrate at $\xi = 0.5$.

The initial average temperature at the instant $t_o = 0$ was assumed to be 300 °C, and the actuator was allowed to cool down to 50 °C due to conduction and free convection. It is clear from these plots that the actuation frequency increases with reducing scale, as predicted by (37). Metals perform better than other classes of materials on silicon having a reasonably high actuation frequency ~1 kHz. Fig. 13(a) and (b) shows similar contours for DLC and PMMA substrates, respectively, at small scale. Metals are capable of actuating at higher frequencies on DLC as compared to Si by about half an order of magnitude.

VIII. Results and Discussion

The achievable temperature difference is a system-dependent design variable, which affects the performance of different material combinations. Therefore, the design space available in the material domain can be better explored for a given temperature difference if a few promising candidates are considered for further analyses. Table II lists the properties of films from different material classes considered for this paper based on their optimal thermomechanical performance [14] on silicon. Table III shows the heat-transfer performance of these films on four different substrates, namely, silicon, DLC, Invar, and PMMA. The properties of these substrates are located at the extremes in the material domain (Young's modulus, thermal-expansion coefficient, and thermal conductivity), and as a result, they provide an indication of the scope for exploration of novel candidates, which can improve the performance.

It is evident from Table III that the materials selection has very little scope for the improvement of thermomechanical performance of the BET actuators. Unlike fluids, the thermal diffusivity of different classes of solid-state materials depends largely on their thermal conductivity due to constant volumetric specific heat ($\sim 10^{6.5}$ J/m$^3 \cdot$ K). Therefore, DLC substrates can be considered for high-frequency actuators owing to their large thermal conductivity, but this has to be compensated by their power index, which is an order of magnitude ($\sim 10^{-4}$ mK/W) less than for silicon and Invar substrates. Zinc is the only candidate which significantly betters conventionally employed aluminum films with an effective and efficient performance irrespective of the substrates considered. Zinc films on DLC substrate have the potential to deliver high work at a high actuation frequency ($W_o = 4.35$ J/m$^3 \cdot$ K^2, $f = 1.2$ kHz), and these have not been considered so far for MEMS actuators.

TABLE II
PROPERTIES OF FILMS OF DIFFERENT MATERIALS CONSIDERED BASED ON THEIR THERMOMECHANICAL PERFORMANCE ON SILICON

S.No	Film	E_2	α_2	ρ_2	K_2	C_2
	Material -2	GPa	μm/mK	kg/m^3	W/mK	J/kg.K
1	Be	303.00	11.50	1850.00	175.00	2178.00
2	Steel	207.00	13.10	7700.00	32.00	490.00
3	Zn	97.00	31.20	7140.00	120.00	390.00
4	Cu	110.00	16.40	8960.00	398.00	385.00
5	Mg	45.00	26.10	1850.00	156.00	1015.00
6	PMMA	2.50	75.00	1190.00	0.20	1500.00
7	PS	3.00	72.50	1045.00	0.12	1700.00
10	PDMS	4.00	60.00	970.00	0.15	1460.00
11	Epoxies	2.00	55.00	1100.00	0.20	1500.00
12	PP	2.00	120.00	900.00	0.12	1900.00
13	Pb	14.00	29.10	1.13X10^4	35	125
14	Ni	207.00	13.10	8900	91	445
15	Ti	110.00	9.00	4540	22	535
16	BeO	345.00	7.00	1850	200	1850
17	Al2O3	370.00	7.40	3870	30	700
18	CI	165.00	12.00	7300	35	540
19	Al	70.00	24.00	2700	237	925
20	Zr_2O_3	200.00	12.00	6050	2	430
21	W	400.00	4.30	19250	178	133
22	B	320.00	8.30	2470	27	1024
23	Nb	105.00	7.30	8600	55	265
24	Ge	102.00	5.75	5323	60	310
25	Si	165.00	2.49	2280	150	700
26	SiO_2	75.00	0.40	2150	1.2	725
27	Si_3N_4	300.00	2.80	3184	30	840
28	DLC	700.00	1.18	3500	1100	518
29	Invar	145.00	0.36	8100	13	510

Zinc films up to a few micrometers can be grown on silicon by sputter deposition [18]. However, despite the potentially superior performance to aluminum, zinc films require cautious evaluation due to their chemically reactive nature.

The electromechanical efficiency of BET actuators is inherently low $(\eta_{\rm em} : 10^{-4})$ due to excess-heat dissipation, and it is an order of magnitude lower than the efficiency of linear (unimaterial) thermal-expansion actuators [8]. This is due to inherently low $W_{\rm o}$ associated with BET actuators [7] as compared to unimaterial thermal-expansion actuators by an order of magnitude for a constant temperature difference. Furthermore, the work associated with electrothermal actuation is always irreversible unlike mechanical actuation. It is evident from Fig. 10 that there is no appreciable variation in the electromechanical efficiency $(\eta_{\rm em} : 10^{-5} - 10^{-6})$ for all the films on the various substrates considered. However, their effectiveness varies significantly. Table IV shows a comparison of the effectiveness indices of different films on various substrates. Engineering polymers are very effective for high-displacement actuators. Candidate materials such as PP, PMMA, PS, and PDMS on Invar and SiO_2 substrates and Zr_2O_3 on PMMA substrate are capable of delivering high displacement per cycle per unit electrical energy consumed $(\Theta_{\rm EI} \sim 10^{-4}$ m/W). Thin polymeric films up to a few tens of micrometers can be achieved by spin coating, which is a proven microfabrication route [19] for growing polymeric films on a substrate. For actuators to deliver a high force per cycle effectively, material combinations such as Zr_2O_3, steel, Zn, Ni on PMMA/Si and Zr_2O_3, steel, Al_2O_3, Ti, Ni, Si_3N_4 on Invar, and Zn on DLC can be considered $(M_{\rm EI} \sim 10^3 - 10^4$ N/Wm). It should be noted again that polymeric substrates require a large thickness to compensate for their low Young's modulus, which may not be acceptable in some applications. Material combinations such as SiO_2 on PMMA and Zr_2O_3, steel, Zn, and Ni on Invar can be considered for actuators to deliver high work effectively $(W_{\rm EI} \sim 10^{-0.08} - 10^{-4}$ N/W^2). It is noteworthy that the most commonly employed material combination Al/Si is bettered by many others for effectiveness. This is due to the high thermal conductivity of aluminum, which causes more heat dissipation despite its favorable mechanical properties.

However, for high-frequency applications, it essential to have high dissipation rate, and therefore, the candidate materials

TABLE III
PERFORMANCE BASED ON HEAT-TRANSFER ANALYSIS FOR DIFFERENT FILMS ON VARIOUS SUBSTRATES

S.No	Film Material-2	Silicon - Material 1				DLC - Material 1				Invar - Material 1				PMMA - Material 1			
		$P_j X10^3$	$[W_n]_o$	f	$\text{Log}_{10}(\eta_{om})$	$P_j X10^4$	$[W_n]_o$	f	$\text{Log}_{10}(\eta_{om})$	$P_j X10^3$	$[W_n]_o$	f	$\text{Log}_{10}(\eta_{om})$	$P_j X10$	$[W_n]_o$	f	$\text{Log}_{10}(\eta_{om})$
		mK/W	Nm/m^3K^2	Hz		mK/W	Nm/m^3K^2	Hz		mK/W	Nm/m^3K^2	Hz		mK/W	Nm/m^3K^2	Hz	
1	Be	2.08	0.42	488	-5.31	6.15	1.10	1373	-4.97	4.21	0.59	155	-5.35	0.23	0.79	60	-4.90
2	Steel	3.53	0.49	287	-5.24	8.17	1.16	1057	-4.93	15.39	0.65	44	-5.29	1.00	0.73	13	-4.94
3	Zn	2.51	2.40	468	-4.48	8.64	4.35	1221	-4.27	4.64	2.62	169	-4.62	0.20	0.33	70	-5.27
4	Cu	1.16	0.60	874	-5.14	5.58	1.23	1597	-4.90	1.52	0.76	464	-5.20	0.06	0.61	208	-5.03
5	Mg	2.17	1.01	690	-4.75	9.61	1.67	1485	-4.56	3.18	1.15	312	-4.88	0.11	0.37	132	-5.20
6	PMMA	20.06	0.98	75	-4.77	53.57	1.14	278	-4.70	197.75	1.02	7	-4.81	16.67	0.00	1	-
7	PS	18.59	1.07	82	-4.72	49.24	1.26	304	-4.66	191.61	1.12	7	-4.78	20.60	0.00	1	-8.16
10	PDMS	16.39	0.93	113	-4.70	43.04	1.12	428	-4.62	168.33	0.98	9	-4.77	18.73	0.02	1	-6.50
11	Epoxies	22.14	0.42	73	-5.10	59.52	0.49	270	-5.04	215.71	0.45	6	-5.14	16.67	0.02	1	-6.42
12	PP	22.24	2.10	70	-4.42	59.60	2.39	260	-4.37	226.19	2.15	6	-4.47	21.13	0.11	1	-5.73
13	Pb	5.47	0.56	335	-4.93	19.97	0.79	911	-4.78	11.19	0.63	116	-5.02	0.32	0.24	50	-5.35
14	Ni	2.73	0.49	360	-5.26	7.47	1.16	1112	-4.95	6.87	0.65	96	-5.30	0.36	0.73	37	-4.95
15	Ti	4.19	0.13	309	-5.70	10.16	0.32	1161	-5.35	18.72	0.22	44	-5.67	1.09	0.77	13	-4.89
16	BeO	1.96	0.11	581	-5.84	5.84	0.38	1653	-5.37	3.85	0.22	179	-5.75	0.21	0.92	66	-4.83
17	Al_2O_3	3.27	0.13	399	-5.69	6.94	0.45	1644	-5.22	17.05	0.25	44	-5.66	1.35	0.91	11	-4.82
18	Cl	3.60	0.35	267	-5.41	8.70	0.82	942	-5.11	14.10	0.49	47	-5.42	0.83	0.74	16	-4.95
19	Al	1.64	1.11	755	-4.79	7.50	1.97	1520	-4.58	2.30	1.28	366	-4.90	0.09	0.43	159	-5.15
20	Zr_2O_3	4.19	0.38	306	-5.24	8.67	0.93	1319	-4.91	41.98	0.54	18	-5.31	8.75	0.75	2	-4.90
21	W	2.07	0.02	651	-6.53	5.80	0.12	2050	-5.79	4.44	0.08	169	-6.14	0.25	1.01	57	-4.77
22	B	3.38	0.18	396	-5.56	7.25	0.54	1638	-5.13	17.89	0.31	43	-5.57	1.40	0.88	10	-4.83
23	Nb	3.43	0.07	392	-5.96	9.61	0.19	1288	-5.56	9.34	0.14	91	-5.86	0.44	0.81	32	-4.87
24	Ge	3.35	0.03	489	-6.22	9.60	0.10	1635	-5.72	8.64	0.08	111	-6.04	0.40	0.84	37	-4.83
25	Si	2.22	0.00	750	-	7.24	0.01	2205	-6.65	4.20	0.02	218	-6.76	0.20	0.98	75	-4.77
26	SiO_2	5.45	0.01	310	-6.67	12.25	0.00	1340	-7.33	54.32	0.00	19	-10.35	9.41	0.93	2	-4.78
27	Si_3N_4	3.37	0.00	384	-8.13	7.35	0.03	1550	-6.45	16.69	0.03	45	-6.61	1.24	1.03	12	-4.77
28	DLC	0.72	0.01	2205	-6.65	3.03	0.00	4842	-	0.94	0.00	827	-7.41	0.05	1.14	278	-4.70
29	Invar	4.20	0.02	218	-6.76	9.44	0.00	827	-7.41	25.64	0.00	25	-	1.98	1.02	7	-4.81

TABLE IV
COMPARISON OF THE EFFECTIVENESS OF DIFFERENT FILMS ON VARIOUS SUBSTRATES

S.No	Film Material-2	Silicon - Material 1			DLC- Material 1			Invar- Material 1			PMMA- Material 1		
		$\log_{10}(W_{EI})$	$\log_{10}(M_{EI})$	$\log_{10}(\Theta_{EI})$	$\log_{10}(W_{EI})$	$\log_{10}(M_{EI})$	$\log_{10}(\Theta_{EI})$	$\log_{10}(W_{EI})$	$\log_{10}(M_{EI})$	$\log_{10}(\Theta_{EI})$	$\log_{10}(W_{EI})$	$\log_{10}(M_{EI})$	$\log_{10}(\Theta_{EI})$
		N/W^2	N / Wm	mW	N/W^2	N / Wm	mW	N/W^2	N / Wm	mW	N/W^2	N / Wm	mW
1	Be	-5.75	2.71	-7.55	-6.38	2.54	-8.02	-4.98	3.07	-7.15	-3.39	3.18	-5.67
2	Steel	-5.22	2.94	-7.25	-6.11	2.63	-7.84	-3.81	3.62	-6.53	-2.14	3.80	-5.03
3	Zn	-4.82	3.05	-6.97	-5.49	2.82	-7.41	-4.25	3.32	-6.67	-3.88	2.91	-5.88
4	Cu	-6.09	2.43	-7.61	-6.42	2.38	-7.89	-5.75	2.58	-7.44	-4.61	2.55	-6.25
5	Mg	-5.32	2.70	-7.12	-5.81	2.54	-7.44	-4.93	2.88	-6.91	-4.34	2.65	-6.09
6	PMMA	-3.41	3.16	-5.66	-4.49	2.64	-6.23	-1.40	4.16	-4.65	-	-	-
7	PS	-3.43	3.18	-5.71	-4.51	2.67	-6.28	-1.39	4.20	-4.68	-2.77	3.25	-5.11
10	PDMS	-3.60	3.15	-5.85	-4.68	2.64	-6.42	-1.56	4.17	-4.82	-1.24	4.04	-4.38
11	Epoxies	-3.69	2.97	-5.76	-4.76	2.46	-6.32	-1.68	3.97	-4.75	-1.24	3.97	-4.30
12	PP	-2.98	3.33	-5.41	-4.07	2.80	-5.97	-0.96	4.34	-4.39	-0.33	4.42	-3.85
13	Pb	-4.78	2.79	-6.66	-5.50	2.48	-7.08	-4.10	3.12	-6.32	-3.61	2.95	-5.66
14	Ni	-5.44	2.82	-7.36	-6.19	2.59	-7.87	-4.51	3.27	-6.88	-3.02	3.36	-5.47
15	Ti	-5.63	2.66	-7.39	-6.48	2.35	-7.92	-4.11	3.40	-6.62	-2.04	3.83	-4.97
16	BeO	-6.38	2.41	-7.88	-6.89	2.31	-8.29	-5.49	2.83	-7.42	-3.39	3.18	-5.67
17	Al_2O_3	-5.84	2.68	-7.62	-6.66	2.43	-8.19	-4.13	3.52	-6.74	-1.78	3.99	-4.86
18	Cl	-5.34	2.85	-7.29	-6.21	2.55	-7.85	-4.01	3.50	-6.61	-2.29	3.71	-5.11
19	Al	-5.52	2.66	-7.28	-5.95	2.54	-7.59	-5.17	2.82	-7.09	-4.48	2.60	-6.17
20	Zr_2O_3	-5.17	2.96	-7.22	-6.15	2.60	-7.85	-3.02	4.01	-6.13	-0.24	4.75	-4.08
21	W	-7.09	2.06	-8.25	-7.40	2.07	-8.57	-5.79	2.69	-7.58	-3.19	3.28	-5.57
22	B	-5.69	2.74	-7.53	-6.55	2.47	-8.11	-4.01	3.57	-6.67	-1.76	3.99	-4.85
23	Nb	-6.08	2.43	-7.61	-6.75	2.21	-8.05	-4.92	3.00	-7.01	-2.80	3.45	-5.35
24	Ge	-6.45	2.24	-7.79	-7.02	2.07	-8.18	-5.21	2.85	-7.16	-2.87	3.42	-5.38
25	Si	-	-	-	-8.20	1.55	-8.85	-6.54	2.24	-7.87	-3.41	3.16	-5.66
26	SiO_2	-6.49	2.18	-7.77	-8.44	1.31	-8.84	-7.95	1.44	-8.49	-0.08	4.80	-3.98
27	Si_3N_4	-8.25	1.45	-8.80	-7.84	1.81	-8.75	-5.11	3.01	-7.21	-1.80	3.97	-4.87
28	DLC	-8.20	1.55	-8.85	-	-	-	-8.41	1.42	-8.93	-4.49	2.64	-6.23
29	Invar	-6.54	2.24	-7.87	-8.41	1.42	-8.93	-	-	-	-1.40	4.16	-4.65

should possess a high thermal conductivity. The optimal material combinations in order to achieve high actuation frequency are DLC/Zn, DLC/Al, DLC/Cu, Si/Zn, and Si/Al. Amorphous DLC films (sp^3 bonded) up to a few micrometers thick can be prepared by pulsed-laser deposition [20], magnetron sputtering with ion plating [21], or a filtered-cathode vacuum arc [22].

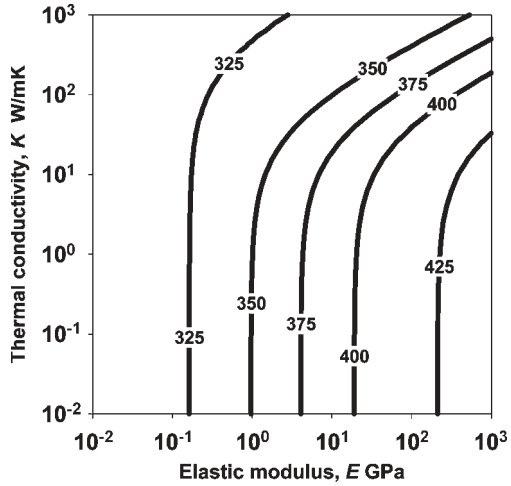

(a)

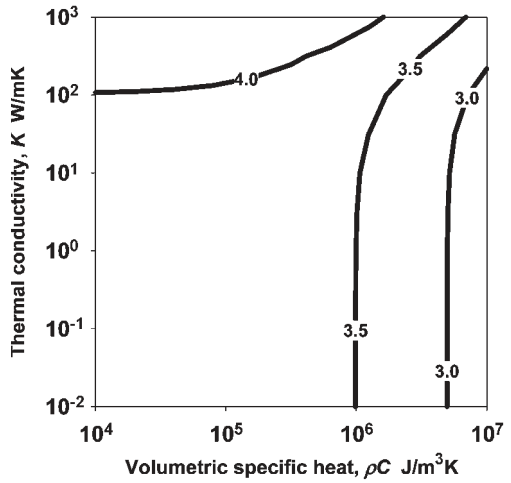

(b)

Fig. 14. Effect of forced convection on (a) steady-state isotherms and (b) actuation frequency for different classes of materials on silicon at small scale ($L = 100$ μm).

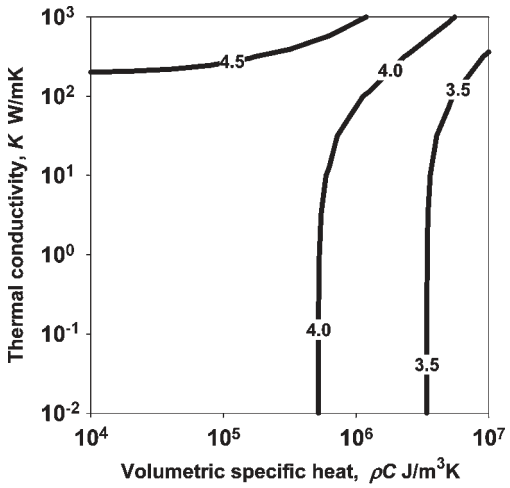

(a)

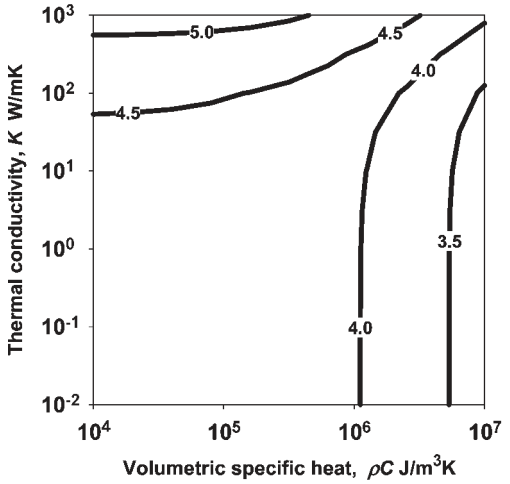

(b)

Fig. 15. Increase in the actuation frequency accomplished by (a) reducing the scale ($L = 60$ μm) and (b) reducing the operating temperature range (573 K–423 K).

A few micrometer-thick aluminum films can be achieved by sputtering [23], [24], which is an established and proven microfabrication route. These material combinations could at best yield $\sim$1.2 kHz for $L = 100$ μm and are limited by the cooling rates achieved by conduction and natural convection at small scales. Frequencies can be further increased if the cooling rate is accelerated by forced convection.

The length scale of the actuator structure is a critical design parameter for applications such as flow-control devices. For a subsonic flow (Mach number, $M = 0.5$), the Knudsen number K_n evaluated at the atmospheric pressure and temperature for a characteristic length $L = 100$ μm is $\sim 10^{-4} (< 10^{-2})$, which ensures that rarefied gas effects can be neglected in the flow analysis [25]. Using von Karman closed-form solutions [26], the average heat-transfer coefficient due to forced convective currents can be evaluated for the bimaterial actuator. Fig. 14(a) and (b) shows isotherms and contours of equal actuation frequency for a range of materials on silicon considering heat dissipation due to conduction and forced convection. Although there is a marginal drop in the steady-state isotherms ($\sim$25 K), the actuation frequency increases by almost an order of magnitude $\sim$7 kHz. Frequencies on the order of $\sim$10 kHz can be achieved for engineering alloys/metals if either the scale is reduced to 60 μm or if the temperature range is restricted to 423 K–573 K. In either case, the work/volume delivered by the actuator per cycle is reduced. Fig. 15(a) and (b) shows the contours of equal actuation frequency for the two cases; $L = 60$ μm and $L = 100$ μm, with the operating temperature range of $\sim$423 K$-$573 K, respectively. Hitherto, piezoelectric actuators [27], [28] and electrostatic actuators [29] have been preferred for applications such as boundary-layer flow-control devices, which operate at high frequencies on the order $\sim$10 kHz. The results presented herein suggest the point at which electrothermal actuators might be considered as viable alternatives.

The ability to achieve mechanical resonance is enabling for many sensor applications, although it may be detrimental for actuator structures. Electrostatic and piezoelectric devices are often operated at resonance. The fundamental mechanical resonant frequencies of bimaterials are therefore estimated using the

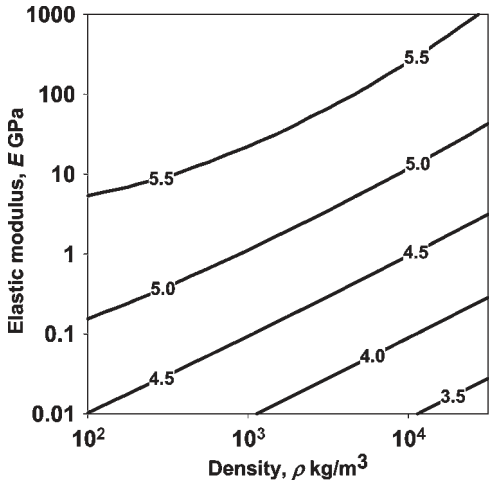

Fig. 16. Contours of equal resonant frequency (fundamental flexural mode) $\log_{10}(f_s)$ for different materials on silicon for an optimal thickness ratio at small scale ($L = 100\ \mu$m).

Euler–Bernoulli relation to compare with the thermal-actuation frequencies. The fundamental structural frequency $f_{\rm s}$ (flexural mode) for a bimaterial structure with an optimal geometry is given as

$$f_{\rm s} = \frac{1}{2\pi}\left(\frac{1.8751}{L}\right)^2 \sqrt{\left(\frac{E_1 t^2}{3\lambda(\rho_1\xi_{\rm o}+\rho_2)(\xi_{\rm o}+1)}\right)} \quad (38)$$

where ρ_1 and ρ_2 are the densities of the bimaterials. Fig. 16 shows contours of equal structural frequency (fundamental flexural mode) for range of materials on silicon plotted in the domain of governing material properties (E versus ρ) for $L = 100\ \mu$m at optimal thickness ratio. It is evident that the structural frequencies are approximately an order of magnitude greater than the thermal-actuation frequencies for different classes of materials at optimal configuration. Thermal-actuation frequencies were found to be always less than the structural frequencies for realistic values of the scales and thickness ratios. If electrothermal actuation was to be considered for high-frequency applications, it would have to be achieved either by using a triggering mechanism or by exploiting nonlinear structural behavior. It should also be noted that, unlike the structural frequency, which is inversely proportional to the actuator length, the thermal actuation frequency is inversely proportional to the square of the actuator length.

IX. Conclusion

The competition between the different modes of heat transfer was studied at various scales using a simple lumped heat-capacity model for a BET actuator. The choice of materials has a significant effect on functional effectiveness and actuation frequencies for the specified temperature limits. BET actuators have the potential to operate at actuation frequencies $\sim$10 kHz at scales less than 100 μm with optimal choices of engineering alloys/metals on Si substrates. DLC substrate can be considered for high-frequency applications such as micromirror positioners, microcage devices, and fiber-optic switches, where high power consumption is permissible. The potential of Invar as a substrate for high force or work at low frequency requiring relatively low power is yet to be realized in microsystems, even though it is promising and should therefore be considered for further research studies. Although polymeric substrates are promising for high-displacement low-frequency applications, their time-dependent nonlinear response requires further consideration. The influence of materials choice on the electromechanical efficiency is very small for BET actuators, and the overall efficiency is inherently very low irrespective of the substrates. Thermally induced mechanical resonance cannot be directly achieved using bimaterial structures with realistic thickness ratios. In addition to the specific results presented herein, we believe that the overall approach to the selection of materials for microsystems is the very outcome of this paper. Applying rational engineering criteria for the selection of materials for new systems and the development of new materials and processes is important to allow the potential of MEMS technology to be fully realized.

References

[1] S. M Spearing, "Materials issues in microelectromechanical systems (MEMS)," *Acta Mater.*, vol. 48, no. 1, pp. 179–196, Jan. 2000.
[2] H. Sehr, I. S Tomlin, B. Huang, S. P. Beeby, A. G. R. Evans, A. Brunnschweiler, G. J. Ensell, C. G. J. Schabmueller, and T. E. G. Niblock, "Time constant and lateral resonances of thermal vertical bimorph actuators," *J. Micromech. Microeng.*, vol. 12, no. 4, pp. 410–413, 2002.
[3] M. Chiao and L. Lin, "Self-buckling of micromachined beams under resistive heating," *J. Microelectromech. Syst.*, vol. 9, no. 1, pp. 146–151, 2000.
[4] J. K. Luo, J. H. He, Y. Q. Fu, A. J. Flewitt, S. M. Spearing, N. A. Fleck, and W. I. Milne, "Fabrication and characterization of diamond-like carbon/Ni bimorph normally closed microcages," *J. Micromech. Microeng.*, vol. 15, no. 8, pp. 1406–1413, Aug. 2005.
[5] N. T. Nguyen, S. S. Ho, and C. L. N. Low, "A polymeric micro gripper with integrated thermal actuators," *J. Micromech. Microeng.*, vol. 14, no. 7, pp. 969–974, Jul. 2004.
[6] L. H. Han and S. Chen, "Wireless bimorph micro-actuators by pulsed laser heating," *Sens. Actuators A, Phys.*, vol. 121, no. 1, pp. 35–43, 2005.
[7] W. P. King, "Design analysis of heated atomic force microscope cantilevers for nanotopography measurements," *J. Micromech. Microeng.*, vol. 15, no. 12, pp. 2441–2448, Dec. 2005.
[8] J. E. Huber, N. A. Fleck, and M. F. Ashby, "The selection of mechanical actuators based on performance indices," *Proc. R. Soc. Lond. A, Math. Phys. Sci.*, vol. 453, no. 1965, pp. 2185–2205, 1997.
[9] D. J. Bell, T. J. Lu, N. A. Fleck, and S. M. Spearing, "MEMS actuators and sensors: Observation on their performance and selection for purpose," *J. Micromech. Microeng.*, vol. 15, no. 7, pp. S153–S164, 2005.
[10] S. Prasanna and S. M. Spearing, "Materials selection and design of microelectrothermal actuators," in *Proc. IET Seminar MEMS Sens. Actuators*, London, U.K., 2006, pp. 260–265.
[11] J. Singh, T. Gan, A. Agarwal, M. Raj, and S. Liw, "3D free space thermally actuated micro mirror device," *Sens. Actuators A, Phys.*, vol. 123–124, no. 1, pp. 468–475, 2005.
[12] M. Hoffmann, P. Kopka, and E. Voges, "Bistable micromechanical fibre optic switches on silicon with thermal actuators," *Sens. Actuators A, Phys.*, vol. 78, no. 1, pp. 28–35, Jan. 1999.
[13] S. Timoshenko, "Analysis of bimetal thermostats," *J. Opt. Soc. Amer.*, vol. 11, no. 3, pp. 233–255, 1925.
[14] S. Prasanna and S. M. Spearing, "Materials selection and design of microelectrothermal bimaterial actuators," *J. Microelectromech. Syst.*, vol. 16, no. 2, pp. 248–259, Apr. 2007.
[15] J. P. Holman, *Heat Transfer*, 9th ed. New York: McGraw-Hill, 2004, pp. 133–135.

[16] J. Y. W. Seto, "The electrical properties of polycrystalline silicon films," *J. Appl. Phys.*, vol. 48, no. 12, pp. 5247–5254, 1975.
[17] *Cambridge Engineering Selector*, 2006. Edupack Ver.4.6.1, GRANTA design Ltd.
[18] G. Perluzzo, C. K. Jen, and E. L. Adler, "Characteristics of reactive magnetron sputtered ZnO films," in *Proc. IEEE Ultrason. Symp.*, 1989, pp. 373–376.
[19] L. Tan, Y. P. Kong, L. R. Bao, X. D. Huang, L. J. Guo, S. W Pang, and A. F. Yee, "Imprinting polymer film on patterned substrates," *J. Vac. Sci. Technol. B, Microelectron.*, vol. 21, no. 6, pp. 2742–2748, 2003.
[20] A. A. Voevodin, M. S. Donley, and J. S. Zabinski, "Pulsed laser deposition of diamond-like carbon wear protective coatings," *Surf. Coat. Technol.*, vol. 92, no. 1, pp. 42–49, Jun. 1997.
[21] J. Schwan *et al.*, "Tetrahedral amorphous carbon films prepared by magnetron sputtering and dc ion plating," *J. Appl. Phys.*, vol. 79, no. 3, pp. 1416–1422, Feb. 1996.
[22] A. C. Ferrari *et al.*, "Stress reduction and bond stability during thermal annealing of tetrahedral amorphous carbon," *J. Appl. Phys.*, vol. 85, no. 10, pp. 7191–7197, 1999.
[23] M. Inoue, K. Hashizume, and H. Tsuchikawa, "The properties of aluminium thin films sputter deposited at elevated temperatures," *J. Vac. Sci. Technol. A, Vac. Surf. Films*, vol. 6, no. 3, pp. 1636–1639, 1988.
[24] D. S. Gardner and P. A. Flinn, "Mechanical stress as a function of temperature in aluminium films," *IEEE Trans. Electron Devices*, vol. 35, no. 12, pp. 2160–2169, Dec. 1988.
[25] R. W. Barber, D. R. Emerson, X. J. Gu, and Y. Zhang, *Rarefied Gas Dynamics in Micro Devices*. [Online]. Available: http://www.cse.clrc.ac.uk/ceg/c4m/rgd.shtml
[26] A. J. Chapman, *Heat Transfer*, 4th ed. New York: Macmillan, 1984, pp. 210–219.
[27] S. A. Jacobson and W. C. Reynolds, "Active control of streamwise vortices and streaks in boundary layers," *J. Fluid Mech.*, vol. 360, no. 1, pp. 179–211, 1998.
[28] T. Segawa, Y. Kawaguchi, Y. Kikushima, and H. Yoshida, "Active control of streak structures in wall turbulence using an actuator array producing inclined wavy disturbances," *J. Turbul.*, vol. 3, no. 1, pp. 1–14, Jan. 2002.
[29] J. R. Frutos *et al.*, "An electrostatically actuated valve for turbulent boundary layer control," *Proc. IEEE Sensors*, pp. 82–88, 2005.

Prasanna Srinivasan received the M.S. degree in mechanical engineering from the Indian Institute of Technology—Madras, Chennai, India, in 2000.

He was a Design Engineer for GE aircraft engines global engineering unit in Bangalore, India, from 2000 to 2003, where he was a member of the structural design team in development engine programs. He is currently a Postgraduate Research Scholar in the Materials Research Group within the School of Engineering Sciences, University of Southampton, Southampton, U.K. His research interests include design and analysis of structures at micro/nanoscales, materials and structures for the design of MEMS devices, mechanics of carbon nanotubes structures, solid mechanics, heat transfer, and fluid flow analysis. He is currently involved in research that focuses on optimal materials selection for improving the performance of MEMS devices.

S. Mark Spearing received the Ph.D. degree from the Department of Engineering, Cambridge University, Cambridge, U.K., in 1990.

Since 2004, he has been a Professor of Engineering Materials in the School of Engineering Sciences, University of Southampton, Southampton, U.K. Prior to this, he spent ten years as a Professor of Aeronautics and Astronautics at Massachusetts Institute of Technology (MIT), Cambridge. His technical interests include materials characterizations and structural analysis and design of MEMS, development of wafer-bonding technologies, microelectronic and MEMS packaging, and advanced composites. From 1995 to 2005, he was responsible for materials, structural design, and packaging tasks of the MIT MicroEngine, MicroRobot, Micro-Chemical Power, and MicroHydraulic Transducer projects as well as conducting cross-cutting underpinning technology development.

Dr. Spearing is an Associate Editor of the JOURNAL OF MICROELECTROMECHANICAL SYSTEM and a member of the American Society of Mechanical Engineers. In 2004, he received a Royal Society Wolfson Research Merit Award.